NANO LETTERS

Letter

pubs.acs.org/NanoLett

Strain and Hole Gas Induced Raman Shifts in Ge−Si_xGe_{1-x} Core−Shell Nanowires Using Tip-Enhanced Raman Spectroscopy

Zhongjian Zhang, David C. Dillen, Emanuel Tutuc, and Edward T. Yu*

Microelectronics Research Center, University of Texas, 10100 Burnet Rd, Building 160, Austin, Texas 78758, United States

Supporting Information

ABSTRACT: We report tip-enhanced and conventional Raman spectroscopy studies of Ge−$Si_{0.5}Ge_{0.5}$ core−shell nanowires in which we observe two distinct Ge−Ge vibrational mode Raman peaks associated with vibrations in the Ge nanowire core and at the Ge−$Si_{0.5}Ge_{0.5}$ interface at which a quantum-confined hole gas is formed. Tip enhanced Raman measurements show dramatically increased sensitivity to the modes at the Ge−$Si_{0.5}Ge_{0.5}$ interface and a shift in position of this mode due to plasmonic field localization at the tip apex and the resulting change in phonon self-energy caused by increased coupling between phonons and intervalence-band carrier transitions.

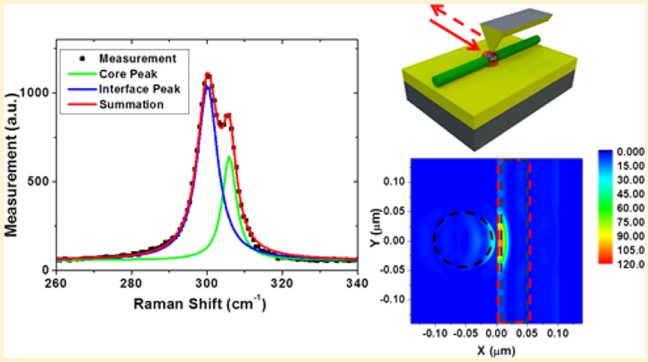

KEYWORDS: *Tip-enhanced Raman scattering, Raman spectroscopy, atomic force microscopy, optical near-field spectroscopy, nanowire, core−shell, heterostructure, germanium, silicon−germanium, strain*

Phonons in solid-state materials are influenced by a broad range of material characteristics, including local bonding configurations, strain, temperature, and the presence of mobile carriers. Raman spectroscopy provides a powerful probe of these and related material properties via scattering of incident light by phonons in the material,[1,2] but is limited in the spatial resolution that can be achieved by the wavelength of the incident light. Tip-enhanced Raman spectroscopy (TERS) allows spatial resolution to be improved over that achieved in conventional Raman spectroscopy by employing a metallic nanostructure at the apex of an atomic force microscope tip to induce plasmonic localization and amplification of incident light in the immediate vicinity of the probe tip.[3−5] Furthermore, the combination of instrumentation for Raman spectroscopy and atomic force microscopy (AFM) in a single measurement apparatus allows information concerning structural, electrical, or other properties that can be probed at the nanoscale using AFM and related techniques to be correlated with that gleaned from TERS measurements that can be performed with similar spatial resolution.

TERS can be particularly useful for semiconductor nanowires and nanowire heterostructures due to the variations in composition, bonding, strain, and carrier density that are present at the nanoscale. Among these, group IV nanowires and nanowire heterostructures are of current interest for a broad range of applications including field-effect transistors with enhanced carrier mobility,[6,7] superconducting devices,[8,9] quantum computing;[10,11] engineered thermal transport,[12,13] and thermoelectrics.[14,15] In Ge−Si_xGe_{1-x} core−shell nanowires, the lattice mismatch between the Ge core and Si_xGe_{1-x} shell provides an opportunity to characterize the correlation between strain and nanowire dimensions at the nanoscale.[16−18] In addition, the valence-band offset at the Ge−Si_xGe_{1-x} interface leads to formation of a quantum-confined hole gas at that interface, and consequently an opportunity to characterize the interactions between optical phonons and intra and intervalence band transitions enabled by the high hole densities present at the Ge−Si_xGe_{1-x} interface, similar to those that have been observed to occur in heavily doped bulk p-type Ge.[19,20]

We have used TERS to characterize, at the nanoscale, strain, interactions between phonons and mobile carriers, and the influence of tip-induced field localization on Raman spectra in Ge−Si_xGe_{1-x} core−shell nanowires. Our results demonstrate that Raman spectra obtained using TERS combined with structural information provided by AFM topographic imaging can be used to characterize strain distributions at the nanoscale in Ge−Si_xGe_{1-x} nanowire core−shell heterostructures as functions of core and shell dimensions. We also observe clear evidence in Raman spectra obtained by TERS of Raman peak shifts associated with interactions between Ge−Ge vibrational modes and intra and intervalence-band transitions within the quantum-confined hole gas at the Ge−Si_xGe_{1-x} interface, with the improved spatial resolution in the radial direction afforded by TERS enabling more detailed characterization and analysis compared to prior observations of asymmetrical broadening of Raman spectra in Ge−Si_xGe_{1-x} core−shell nanowires.[21] Finally, we combine computational modeling with TERS measurements to demonstrate that proximity of a metallized probe tip

Received: January 15, 2015
Revised: May 4, 2015
Published: June 8, 2015

DOI: 10.1021/acs.nanolett.5b00176
Nano Lett. 2015, 15, 4303−4310

during the TERS measurements leads to alterations in the spatial distribution of the excitation field that enhance phonon-carrier interactions and increase the Raman peak shift associated with these interactions as the probe tip is brought into close proximity to the nanowire surface.

Nanowire samples were grown on Si (111) wafers using Au nanoparticles as catalysts for vapor liquid solid (VLS) growth of the Ge nanowire cores.[22] During VLS growth, the nanowires taper from base to tip due to a small amount of conformal chemical vapor deposition of Ge on the existing nanowire which results in a core thickness that ranges from 35 to 55 nm. After growth of the Ge core, epitaxial shell growth was done using an ultrahigh-vacuum chemical vapor deposition (UHVCVD) process. Typical nanowires were ~6 μm long with the nanowire core axis along the [111] direction. Nanowire dimensions and compositions were verified using transmission electron microscopy (TEM) and energy dispersive X-ray (EDX) spectroscopy.[23] Figure 1a shows a TEM image of

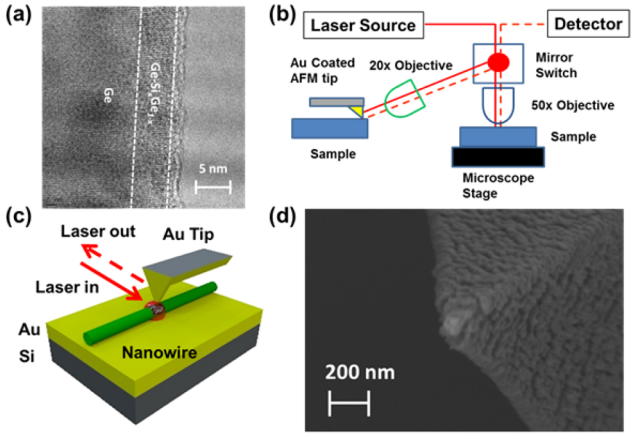

Figure 1. (a) TEM image of Ge−Si$_x$Ge$_{1-x}$ core−shell nanowire. (b) Schematic diagram of TERS and conventional Raman measurement schemes. (c) Schematic diagram of our TERS experimental geometry for TERS measurements of Ge−Si$_{0.5}$Ge$_{0.5}$ core−shell nanowires. (d) SEM image of Cr/Au coated AFM tip used for TERS measurement.

the core−shell nanowire that confirms constant shell thickness and high overall growth quality (for SEM cross section of the nanowire growth and an additional TEM image of nanowire lattice fringes, see Supporting Information, Figure SF1). The Si$_x$Ge$_{1-x}$ shell has a smaller lattice constant than the Ge core; therefore the core region is compressively strained. For the core and shell dimensions and compositions employed here, all the nanowire heterostructures are expected to be coherently strained, based on a prior analysis of strain energetics,[24] with the Ge core region being under compressive strain in both the axial and radial directions.

Parts b and c of Figure 1 show schematic diagrams of the conventional Raman and TERS experimental setups and the tip and sample geometry for the TERS measurements. In preparation for TERS measurements, the Ge−Si$_{0.5}$Ge$_{0.5}$ core−shell nanowires were released from the Si (111) growth substrate by sonicating in ethanol, and dispersed on an Au-coated SiO$_2$/Si (001) substrate by drop casting. The 100 nm thick Au layer blocks any signal from the underlying SiO$_2$ and Si layers. Conventional Raman measurements were obtained using a Horiba Jobin Yvon LabRAM confocal Raman system with a backscattering geometry. For TERS measurements, an AIST-NT Omegascope atomic force microscope coupled to the Horiba Raman measurement apparatus using a system of external mirrors and lenses to align the laser with the probe tip was employed. Nanowires characterized by TERS are first located by AFM topographic scanning, which is also used to determine their diameter (for an AFM image and height profile of a typical nanowire, see Supporting Information, Figure SF2). Diameter measurements were also confirmed using scanning electron microscopy (SEM). The AFM probe tips used for TERS were Si tips with the visible apex of the tetrahedral tip located at the end of the cantilever, and were coated with a metal bilayer consisting of 35 nm Cr/140 nm Au using electron beam deposition. Figure 1d shows a SEM image of a Cr/Au-coated probe tip, from which we deduce that the radius of curvature of metallized probe tips used in the TERS measurements is approximately 50 nm. TERS measurements were performed with the AFM operating in intermittent contact mode with an oscillation amplitude ranging from 3 to 20 nm.

In order to probe the intrinsic nanowire resistivity without contributions from a finite contact resistance, electrical measurements were performed on a back-gated four-point device with 54 nm SiO$_2$ dielectric and boron implanted regions under Ni contacts (the nanowire channel remains undoped, see Supporting Information, Figure SF4, for four-point measurements). Results yield a room temperature conductance of 1.39 × 10^{-5}A/V at zero gate voltage, and a field-effect mobility of 600 cm^2/V·s for a device with channel length of 1100 nm, Ge core diameter of 42 nm, and Si$_{0.5}$Ge$_{0.5}$ shell thickness of 5 nm. The field-effect mobility was extracted using the gate dependence of the intrinsic conductance: $\mu = (dG/dV_{bg})L_{ch}/C_{ox}$, where C_{ox} = 5.56 × 10^{-13} F/cm is the back-gate capacitance per unit length as determined by Sentaurus TCAD simulations (Synopsys). The dependence of conductance on gate voltage indicated that the nanowires are p-type, and the measurement of conductance at zero gate bias combined with Sentaurus TCAD simulations yields a peak hole concentration near the interface of 2 × 10^{18} cm^{-3} (see Supporting Information, section S2, for detailed simulation results).

Figure 2 shows Raman spectra for the Ge−Ge vibrational mode obtained from Ge−Si$_{0.5}$Ge$_{0.5}$ core−shell nanowire

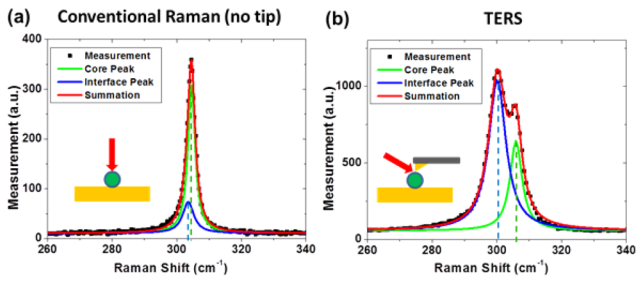

Figure 2. Raman spectra from (a) conventional Raman measurements and (b) TERS measurements. Both spectra are fitted to two Lorentzian peaks: one in green for the core region and one in blue for the interface region. The sum of the two peaks is shown in red in both plots, and shows excellent agreement with the measured spectra.

heterostructures both using the conventional Raman spectroscopy apparatus and via TERS. In each case, the spectra are fitted to two Lorentzian peaks. One peak, shown in green, corresponds to Ge−Ge vibrational modes in the Ge core of the nanowire. The other, shown in blue, is associated with Ge−Ge

DOI: 10.1021/acs.nanolett.5b00176
Nano Lett. 2015, 15, 4303−4310

vibrations in the Ge nanowire core region near the Ge–$Si_{0.5}Ge_{0.5}$ interface, at which a quantum-confined hole gas is present. Prior studies of Raman spectra in heavily doped p-type Ge have demonstrated that coupling between the Ge–Ge vibrational mode and intra- and intervalence-band transitions leads to an asymmetric broadening of the Ge–Ge Raman peak as well as a shift in peak position to smaller wave numbers.[19,20] In addition, behavior similar to that shown in Figure 2a has been observed in earlier Raman spectroscopy studies of Ge–Si core–shell nanowires, and attributed to a superposition of Raman peaks from the Ge nanowire core and the vicinity of the quantum-confined hole gas at the core–shell interface.[21]

In comparing the conventional and tip-enhanced Raman spectra shown in Figure 2, we observe that the amplitude of the peak attributed to Ge–Ge vibrational modes near the core–shell interface (hereafter referred to as the "interface peak") is substantially larger, compared to the peak associated with Ge–Ge vibrations in the Ge core (hereafter referred to as the "core peak"), in the TERS measurement, indicating that TERS yields a stronger relative signal from the interface region. In addition, the separation between the core and interface peaks is significantly greater in the TERS measurement than in the conventional Raman spectrum. We attribute the increase in peak separation in the TERS measurement to an enhancement in coupling between the Ge–Ge vibrational mode and a combination of intra and intervalence-band transitions that occur due to the altered spatial distribution of the electromagnetic field in the vicinity of the probe tip under laser illumination.

Figure 3a shows a schematic band edge energy diagram of the nanowire heterostructure. The interface region in the Ge core contains a two-dimensional hole gas (2DHG) with a much higher hole concentration than in the rest of the core. Based on electrical measurements and transport simulations, a peak carrier density of approximately 2×10^{18} carriers cm^{-3} occurs

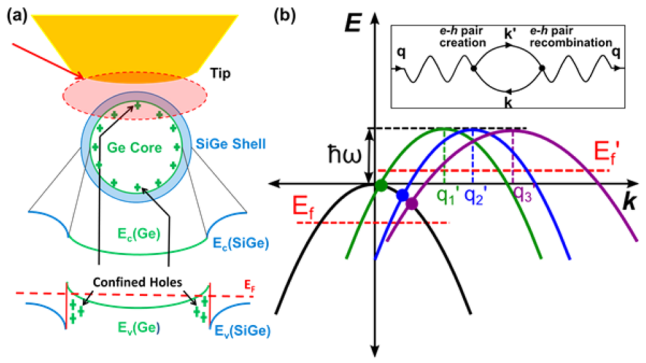

Figure 3. (a) Schematic diagram of the nanowire bandstructure as it relates to the TERS experimental setup. (b) Schematic band diagram showing energy and momentum conservation constraints for the carrier transitions within the valence band. The black parabola represents the initial band dispersion with an initial Fermi level position, E_f. The colored parabolas represent the shift in energy, $\hbar\omega$, and shifts in momentum, q_1', q_2', and q_3', caused by different carrier transitions with the Fermi level at E_f'. The green and blue parabolas indicate intravalence band transitions with two different momentum shifts, q_1' and q_2'. The purple parabola with a shift in momentum q_3' represents a intervalence band transitions between bands with different band curvatures. The inset shows a schematic diagram of the phonon mediated *e-h* pair creation and recombination that alters the self-energy of the phonon.

in the interface region, which is below the threshold in p-type bulk Ge for observing either a red shift in peak position or a broadening in the peak when compared to intrinsic bulk Ge.[19,20] However, the geometry of the 2DHG in the interface region of the nanowire results in a significantly altered valence-band structure, compared to the bulk case, where factors such as the greater curvature of the first and second heavy hole subbands would result in a greater number of occupied and unoccupied valence states near the Fermi energy. A greater number of occupied and unoccupied states near the Fermi energy would allow for coupling between intra and intervalence-band carrier transitions and the Ge–Ge phonon mode comparable to that of much more heavily doped bulk Ge, which would be observed through the similar peak shift and broadening of the Ge–Ge mode Raman peak (see Supporting Information, section S2, for more details).

The shift and broadening of the Raman peak in heavily p-type Ge can be explained by considering the phonon excited in the Raman scattering process and the interaction with 2DHG at the core–shell interface through particle-vacancy creation and recombination processes. For simplicity we illustrate this interaction in Figure 3b for the case of a nondegenerate parabolic band; a quantitative description should take into account the degeneracy and full dispersion of the Ge valence band including confinement effects. For a process of particle-vacancy creation through phonon absorption the energy and momentum conservation conditions may be written as

$$\hbar\omega = \frac{\hbar^2 k'^2}{2m} - \frac{\hbar^2 k^2}{2m} \tag{1}$$

$$\mathbf{k}' = \mathbf{k} + \mathbf{q} \tag{2}$$

respectively, where ω is the phonon frequency, $\mathbf{k}$ and $\mathbf{k}'$ are the wavevectors for the initial and final electronic states, $\mathbf{q}$ is the phonon wave vector, and m is the hole effective mass. Assuming plane wave incident and scattered radiation, the phonon wave vector $\mathbf{q}$ is given, due to momentum conservation, by[20]

$$q = \frac{4\pi}{\lambda} n(\lambda) \tag{3}$$

where λ is the free-space wavelength of the incident light and $n(\lambda)$ is the refractive index of the nanowire material as a function of wavelength. Coupling of phonons to electronic transitions between valence-band states can occur through the deformation potential mechanism, which is directly responsible for the self-energy of the phonons.[20,25] When the phonon frequency is comparable to the free-carrier redistribution time, as is the case for optical phonons that are of interest here, the electron–phonon interaction must be treated quantum mechanically, and can allow for the decay of phonons into hole excitations within the valence bands.[26] These free-particle excitations take place due to transitions of electrons from occupied to unoccupied valence-band states near the Fermi energy. If (i) both interacting elementary excitations are Raman active, as is the case with transverse optical (TO) phonons and electron–hole pairs, (ii) the phonon energy coincides with the energy of the electronic excitations, and (iii) momentum conservation among the phonon momentum and the initial and final electronic state momenta is satisfied, the Raman peak associated with the phonon mode may broaden asymmetrically due to the Fano effect.[20]

In general, Fano resonances arise due to interference between the scattering amplitudes from a discrete excitation

DOI: 10.1021/acs.nanolett.5b00176
Nano Lett. 2015, 15, 4303–4310

and a continuum of transitions,[27] which in this case are the optical phonon and the continuum of electronic transitions within the Ge valence band, respectively. In Raman measurements, coupling between phonons and such transitions can occur when both energy and momentum conservation are satisfied, which in turn requires very high hole concentrations. Figure 3b shows a schematic illustration of the momentum and energy conservation constraints on carrier transitions within the valence band. A carrier transition shifts the energy and momentum of the initial parabolic valence band dispersion, shown in black with Fermi energy E_f, to a new position, shown with the colored parabolas with Fermi energy E_f', depending on the phonon frequency, ω, and wavevector, q. A carrier transition is allowed if the intersection point of the original parabola and the shifted parabola is higher in energy than E_f, which indicates an initially occupied hole state, and lower in energy than E_f', which indicates a final vacant hole state. The energy and momentum conservation constraints for allowed transitions apply to both intra and intervalence-band transitions with changes in dispersion of the bands for the initial and final states implicitly modeled within the allowed intersection points of the original and final parabola. For Ge−Si_xGe_{1-x} core−shell nanowires, the elevated hole concentration in the quantum-confined hole gas, combined with changes in valence-band dispersion in this region, leads to coupling of phonon interactions with a continuum of intervalence-band transitions to produce a shift in the Ge−Ge interface Raman peak. Although the Fano resonance line shape can in principle differ dramatically from the Lorentzian form, we continue to model the Raman spectra for the core−shell nanowires using a superposition of Lorentzian lineshapes as we observe only very limited departures from Lorentzian behavior experimentally, as is evident from Figure 2. The limited asymmetry observed in our measurements is consistent with Raman spectra reported for heavily doped bulk p-type Ge with room temperature hole concentrations similar to those estimated for the quantum-confined hole gas region in our samples.[19,20]

Coupling of phonons to intervalence-band carrier transitions has been identified previously as the dominant mechanism leading to a substantial negative shift in Raman peak wavenumber in heavily doped p-type Ge and Si.[20,28] Intra-valence-band transitions, which may also occur but are not the primary contributor to the observed Raman peak shift, lead to a positive shift in Raman peak wavenumber in heavily doped p-type Ge, as well as a dependence of peak position on the excitation radiation wavelength.[20] Specifically in the case of heavily doped p-type Si, a detailed analysis has shown that coupling of the Si−Si vibrational mode to a continuum of electronic excitations produced by intervalence-band transitions with energies overlapping that of the vibrational mode leads to a shift of the Si−Si Raman peak to smaller wave numbers.[28] The valence band structure of Si is similar in a number of key respects to that of Ge, including splitting that occurs at the top of the valence band under strain, and similar effective masses for both the heavy-hole ($0.49m_e$ and $0.33m_e$ for Si and Ge, respectively, where m_e is the free electron mass) and light-hole ($0.16m_e$ and $0.043m_e$ for Si and Ge, respectively) valence bands.[19] The spin−orbit splittings (0.044 and 0.29 eV for Si and Ge, respectively) differ significantly, but the split-off band is not expected to play a very significant role at the hole concentrations expected to be present in Ge−$Si_{0.5}Ge_{0.5}$ core−shell nanowires.

Because of these similarities between the valence-band structures for Si and Ge, we have adopted the approach of Cerdeira et al.[28] to analyze coupling between Ge−Ge phonon modes and intervalence-band transitions near the Ge/$Si_{0.5}Ge_{0.5}$ interface of the core−shell nanowires employed here. Specifically, the shift in the position of the Ge−Ge Raman peak arising from coupling to intervalence-band transitions is assumed to be given by[28]

$$\hbar\Gamma(\omega) = \pi \int \rho(\hbar\omega)\langle|\langle\psi_i|H|\phi\rangle|^2\rangle_{av}\, dV \tag{4}$$

where Γ is the magnitude of the shift in Raman peak position, $\rho(\hbar\omega)$ is the joint density of states for the continuum of intervalence-band transitions, $\langle|\langle\psi_i|H|\phi\rangle|^2\rangle_{av}$ is the square of the magnitude of the electron−phonon interaction matrix element, averaged over different symmetry directions, and the integral is computed over the nanowire crystal volume. As the Fermi level moves deeper into the valence band with increasing hole concentration, the wave vectors of the optical phonons in a conventional Raman measurement, as given by eq 3, begin to allow electronic excitations within the valence band of p-type Ge at the optical phonon energy.[20] These transitions lower the electronic contribution to the free energy of the material, decreasing the elastic constants and thereby reducing the phonon energy. This behavior is directly observable as a shift of the Raman peak for the Ge−Ge vibrational mode to smaller wave numbers.[19,20]

In a TERS measurement, the proximity of the sample to the metallized AFM probe tip changes the spatial distribution of the electromagnetic field in the sample region near the tip, and consequently increases the coupling between the Ge−Ge vibrational mode and the continuum of intervalence-band transitions. Figure 4 shows computational electromagnetic

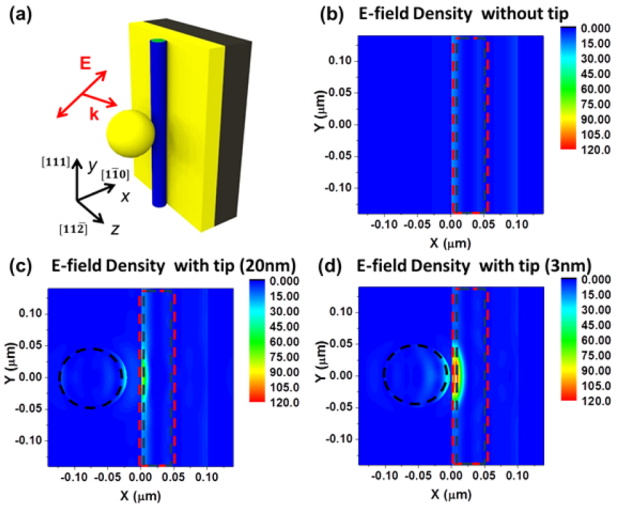

Figure 4. Computational electromagnetic simulations for an electromagnetic plane wave incident on a nanowire in proximity to an AFM probe tip, modeled as an Au sphere. (a) Schematic of simulation geometry showing **k** propagating at an angle of 30° relative to the *z*-axis and the electric field polarized at an angle of 30° relative to the *x*-axis. Spatial cuts of E_x are taken along the center of the nanowire in the *x*−*y* plane. Shown are field distributions for (b) the case without the tip, (c) the case with the tip at a distance of 20 nm from the nanowire, and (d) the case with the tip at a distance of 3 nm from the nanowire. The dashed lines show the position of the tip (modeled as a sphere) and the nanowire.

DOI: 10.1021/acs.nanolett.5b00176
Nano Lett. 2015, 15, 4303−4310

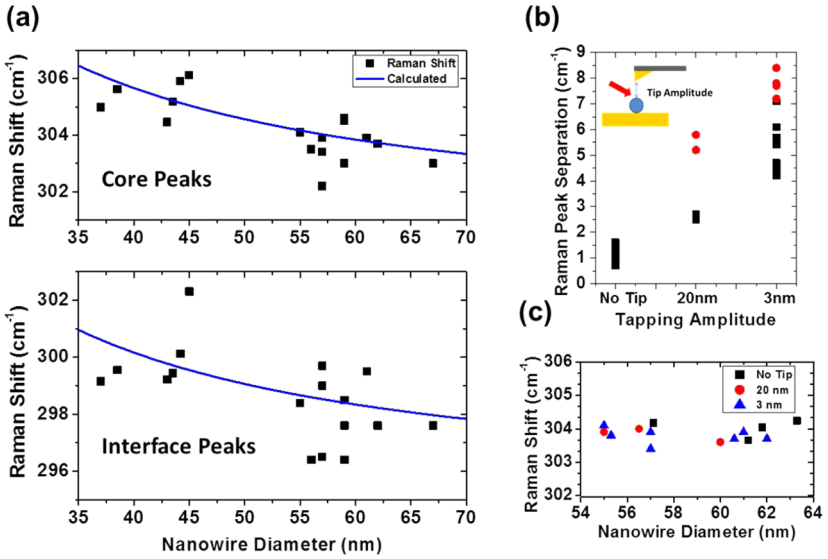

Figure 5. (a) Raman peak positions vs total nanowire diameter. The top panel shows the core peak positions. The calculated Raman shift is shown with the solid blue line. The bottom panel shows the interface peak positions. The solid blue line represents the calculated Raman shift for the core peak (shown in the top panel) rigidly shifted by −5.5 cm^{-1}. (b) Separation between the core and interface peaks for our three measurement conditions. Different symbols represent measurements from different probe tips. (c) Core peak positions for various measurement configurations for a diameter range of 55 to 64 nm. Core peak positions are independent of measurement configuration.

simulations of electric field distributions for a Ge−$Si_{0.5}Ge_{0.5}$ core−shell nanowire with a shell thickness of 5 nm and total diameter of 50 nm positioned just below a metallized probe tip, modeled for simplicity as an Au sphere 100 nm in diameter, and subjected to plane-wave illumination at a wavelength of 633 nm. The simulation geometry is illustrated in Figure 4a. The incident electric field polarization is taken to be normal to the nanowire axis. Prior studies[21] and our own simulations have shown that the polarization of the electric field can substantially influence the amplitude of the field within the nanowire core (see Supporting Information, Figure SF5), and the polarization employed for the simulations shown in Figure 4 was chosen to highlight the effects of field localization by the metallized probe tip. Optical parameters for the materials present in the simulation volume were taken from the literature.[29]

Parts b−d of Figure 4 show plots of the numerically simulated electric field density $U_E(\mathbf{r})$, given by

$$U_E(\mathbf{r}) = \frac{1}{2}\mathrm{Re}[\varepsilon(\mathbf{r})]|\mathbf{E}(\mathbf{r})|^2 \quad (5)$$

where $\varepsilon(\mathbf{r})$ is the complex dielectric function at the appropriate wavelength and $\mathbf{E}(\mathbf{r})$ is the electric field amplitude, in the *xy* plane that bisects the nanowire in the absence of the probe tip, and for separations between the tip and nanowire of 20 and 3 nm. The dashed lines indicate the positions of the Au sphere and the core and shell nanowire regions. As shown in the figure, there is a substantial enhancement in the electric field density in the nanowire region near the Au sphere used to model the metallized AFM probe tip, with the enhancement being much more pronounced, and extending farther into the nanowire, at a tip−sample distance of 3 nm compared to that at 20 nm. In addition, the field distribution in the absence of the Au sphere is, as shown in Figure 4b, largely plane wave-like, whereas with the Au sphere present, as in Figure 4, parts c and d, the field distributions deviate substantially from those for simple plane waves.

The increased field density in the immediate vicinity of the probe tip results in an increased amplitude for the interface peak in the Raman spectra measured by TERS, as is shown in Figure 2. As a result, the positions of both the core and interface peaks can be precisely determined. Figure 5a shows the core and interface Raman peak positions from TERS spectra obtained for several different nanowire regions as functions of total nanowire diameter at the probe tip position. Measurements were performed on regions of Ge−$Si_{0.5}Ge_{0.5}$ core−shell nanowires with diameters ranging from 35 to 70 nm and constant shell thicknesses of 5 nm. All measurements shown in Figure 5a were performed in intermittent contact mode with a tip oscillation amplitude of 3 nm. The solid lines in Figure 5a correspond to Ge−Ge Raman peak positions calculated based on measured nanowire dimensions and assuming coherent strain between the nanowire core and shell. Specifically, the calculated position of the core peak, corresponding to the solid line in the upper plot of Figure 5a, was obtained as a function of nanowire diameter by solving the secular equation of lattice dynamical theory with appropriate elastic constants (see Supporting Information, section S3, for more detailed discussion). The calculated position of the interface peak, corresponding to the solid line in the lower plot of Figure 5a, was obtained by applying a rigid shift of −5.5 cm^{-1} to the calculated core peak positions. For simplicity, this rigid negative shift was determined by taking the average difference between the core and interface peak positions for each individual measurement.

As seen in Figure 5a, the calculated core and interface peak positions, and their dependence on total nanowire diameter, are in good agreement with those measured experimentally. The good agreement between the calculated and measured core peak positions provides confirmation that, for all the nanowire regions studied, the core and shell are coherently strained, with decreasing total nanowire and core diameter leading to an overall shift of the core peak from the intrinsic unstrained Ge−Ge vibrational mode position of 300.5 cm^{-1} to larger wave numbers. This occurs because for a constant shell thickness, it is energetically favorable for compressive strain in the core region to increase in magnitude with decreasing core diameter

DOI: 10.1021/acs.nanolett.5b00176
Nano Lett. 2015, 15, 4303−4310

and consequently volume, leading to the observed increase in Raman peak wavenumber with decreasing nanowire diameter. The very similar diameter dependence of the core and interface Raman peak positions indicates that both the core and interface peak positions are influenced by the same strain configuration. Since the only region of the core−shell nanowire that is expected to have spatially uniform strain is the Ge core, and since the shell region is expected to have a very different strain configuration, with a different diameter dependence, compared to the core,[23] we conclude that both the core and interface peaks are associated with Ge−Ge vibrations in the Ge core, with the interface peaks corresponding to Ge−Ge vibrations near the Ge−$Si_{0.5}Ge_{0.5}$ core−shell interface.

Figure 5b shows the separation between the core and interface peaks measured for various nanowire regions using conventional Raman spectroscopy ("no tip"), and for tip oscillation amplitudes, which to a reasonable approximation correspond to the average distance between the tip apex and sample surface, of either 20 or 3 nm. The two different symbols represent measurements with two different tips. For both probe tips, the separation between the core and interface peaks increases in the presence of the probe tip and as the probe tip moves closer to the sample surface, although the size of the peak separation varies from one tip to the other. Experimental data obtained with a vertical polarizer along the excitation laser path shows the relationship between peak separation and distance between probe tip and sample surface (see Supporting Information, Figure SF9). Figure 5c shows the position of the Raman core peak measured in the absence of a probe tip and for tip oscillation amplitudes of 20 and 3 nm, for nanowire diameters ranging from 55 to 64 nm. The position of the core peak is seen to be independent of proximity to, and even the presence of, the probe tip, demonstrating that the increased peak separation with increasing tip proximity shown in Figure 5b is due entirely to a shift in the position of the interface peak. In addition, the observation that the core peak position remains fixed for the different measurement configurations employed confirms that the enhanced fields from the tip are not significantly changing the background hole density in the Ge core or inducing local heating effects, which would be expected to be more prominent in the TERS measurement than in conventional Raman spectroscopy, and which would produce a negative shift in Ge−Ge core peak position, or introducing other factors that would affect the core peak position.

The shift in Ge−Ge interface peak position with increasing proximity to the probe tip can be explained as follows. Without the Au-coated probe tip present, the phonon wave vector magnitude q, given by eq 3, is determined by the wavelength of the incident illumination and the nanowire refractive index. For typical wavelengths, q is very small in comparison to the size of the Ge crystal Brillouin zone, and therefore severely constrains the intervalence-band transitions that are consistent with conservation of linear momentum. In conventional Raman spectroscopy of a Ge−$Si_{0.5}Ge_{0.5}$ core−shell nanowire, the high hole concentration present in the quantum-confined hole gas at the Ge−$Si_{0.5}Ge_{0.5}$ interface, combined with altered valence-band dispersion associated with quantum confinement, enables these transitions to occur and produces the observed shift in the position of the interface peak position. In the presence of the probe tip, however, the fields are no longer plane wave-like in the immediate vicinity of the tip. The fields scattered by the tip contain additional Fourier components, which provide additional options to satisfy momentum conservation constraints in phonon scattering, and therefore enable greater interaction between the Ge−Ge vibrational modes excited by the incident illumination and electronic transitions within the Ge valence bands. This basic concept was illustrated in Figure 3b, which shows the energy and momentum shifts associated with multiple intra and intervalence-band transitions with the same energy, but different wave vectors; more such transitions will be allowed for TERS compared to conventional Raman measurements.

Fourier analysis of numerically simulated electromagnetic field distributions provides further insight into the influence of probe tip proximity on Raman scattering processes and coupling between optically excited phonons and intervalence-band transitions in the TERS experiments reported here. Specifically, two-dimensional fast Fourier transforms (FFTs) have been performed on the x-component of the electric field, E_x, computed for an electromagnetic plane wave of wavelength 633 nm incident on a Ge−SiGe core−shell nanowire under the same conditions and for the same geometries as in Figure 4. E_x was selected for this analysis because it is the dominant field component in the electric field density in the vicinity of the probe tip (see Supporting Information, Figure SF6). As shown in Figure 6a, the FFT analysis was performed for a 25 nm × 50 nm region of the nanowire closest to the Au sphere in the simulation, and in the xy-plane bisecting the nanowire (see Supporting Information, Figure SF7, for full two-dimensional FFTs). Figure 6b shows the Fourier amplitude as a function of k_y computed from the electromagnetic simulations for $k_x = 0$ in the absence of the Au sphere, corresponding to a conventional Raman spectroscopy measurement configuration, and with the sphere surface either 20 or 3 nm from the nanowire surface, corresponding to TERS measurements with tip oscillation amplitudes of 20 or 3 nm, respectively. Since the allowed wave vectors for carriers in the quantum-confined hole gas in the xy-plane are quantized in the x-direction, the Fourier amplitudes are analyzed only as a function of k_y. The greater Fourier wave amplitudes are limited to k_y values close to the Brillouin zone center, which allows us to assume that the additional Fourier components only create discrete states at the flat zone center region of the Ge optical phonon dispersion and therefore limits the energy range of the optical phonons that interact with the continuum of intervalence-band transitions.

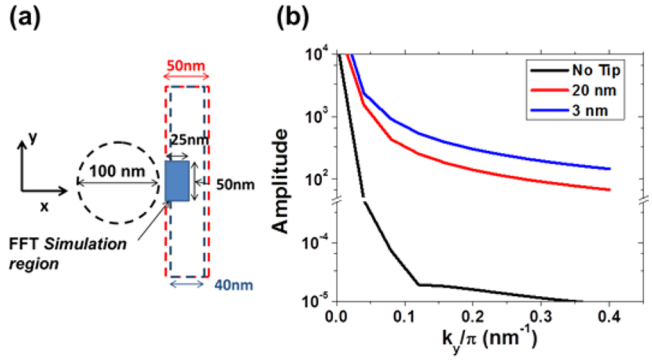

Figure 6. (a) Schematic of the simulation region used to compute the 2D FFT. The calculated electric field component in the x-direction (E_x) for the 25 nm × 50 nm region of the nanowire closest to the Au tip is used to compute the 2D FFT. (b) Fourier amplitude as a function of k_y computed from EM simulations for $k_x = 0$.

DOI: 10.1021/acs.nanolett.5b00176
Nano Lett. 2015, 15, 4303−4310

We model the effect of these additional Fourier components by including multiple discrete phonon states with wavevectors limited to values near the center of the Brillouin zone, consistent with Fourier analysis of simulated field distributions (see Supporting Information, Figure SF7) that interact with the continuum of intervalence-band carrier transitions. The energy range of the optical phonons remains very narrow because the optical phonon dispersion in Ge is nearly flat at the Brillouin zone center.[30] The limited range of energies and wavevector values for the optical phonons results in consistent magnitude of second-order coupling between each discrete phonon state and other excited phonon states, due to coupling via the continuum of carrier transitions, and between each discrete phonon state and the continuum, which combined cause an absolute shift in the phonon self-energy that is consistent across all the discrete states.[27] The consistent absolute shift in the phonon self-energy results in a greater separation between the core and interface peaks with limited peak broadening for the interface peak as can be seen in Figure 5b (see Supporting Information, section S5, for detailed discussion and analysis).

Although the detailed analysis of the additional Raman shift arising from coupling of phonons to intervalence-band transitions was performed assuming bulk valence band structure parameters for Ge, we expect that the same concepts, with qualitatively similar conclusions, should apply for core−shell nanowires and intervalence-band transitions in the quantum-confined hole gas. In particular, we anticipate that coupling between the Ge−Ge vibrational mode and intervalence-band transitions in the quantum-confined hole gas will still occur due to the high local hole concentration, although the strength of that coupling will vary depending on the detailed structure of the valence subbands. The additional Fourier components of the electric field induced by proximity to the probe tip will increase this coupling, just as in the bulk case, resulting in an increased shift of the Raman interface peak to smaller wave numbers in the presence of the probe tip, and with decreasing distance between the probe tip and nanowire surfaces.

In conclusion, we have performed TERS and conventional Raman spectroscopy measurements on Ge-SiGe core−shell nanowires and, for the first time, identified two clearly distinguishable Ge−Ge vibrational mode Raman peaks from the core and interface regions of the nanowires. We confirm the origin of the two Ge−Ge mode Raman peaks, and determine the local strain configuration in the nanowire, through analysis of the diameter dependence of the Raman peak positions. We also demonstrate that positioning the Au coated AFM probe in close proximity to the nanowire directly causes a pronounced increase in the separation between the core and interface peaks and overall larger interface peak signal that indicates localized probing of that specific radial region of the nanowire. By performing a Fourier analysis on electromagnetic simulations of field distributions arising from the presence of a probe tip and the interaction between tip and nanowire, we find an increase of the higher-order Fourier amplitudes in the vicinity of TERS probe. The increased amplitudes of higher-order Fourier components cause significantly more coupling of intervalence-band transitions to phonon modes, which directly leads to an increased negative shift in the position of the interface peak. This study also opens up possibilities for further investigations into local bonding, phonon behavior, carrier distributions, and phonon-carrier interactions in a variety of solid-state nanostructures.

Methods. For nanowire growth, a 7 Å thick Au layer was deposited using electron beam metal deposition on Si(111) wafer after removing the native oxide using dilute hydrofluoric (HF) acid. The wafer was then placed in a cold wall UHV growth chamber and annealed for 15 min in H_2 ambient at ∼370 °C to produce Au nanoparticles catalysts. The Ge nanowire cores were grown using a VLS process at a substrate temperature of ∼280 °C using a GeH_4 (20.8% in He, 50 sccm) precursor at 2.5 Torr. Because of the nonzero radial Ge growth during the VLS process, slight tapering of the Ge core occurs from base to tip. The Ge−Si_xGe_{1-x} shell was then grown epitaxially in situ on the Ge core using a UHVCVD process at ∼380 °C with GeH_4 (20.8% in He, 5 or 10 sccm) and SiH_4 (100%, 50 sccm) precursors at a total chamber pressure of 40 mTorr. Nanowire imaging and EDX measurements were carried out using a JEOL 2010F TEM.

All Raman spectroscopy measurements were performed using laser excitation that is dominated by vertically polarized light at a wavelength of 633 nm. For conventional Raman measurements done using the standard microscope, the laser was focused using a 50× objective for a spot size of ∼2 μm with an incident laser power of ∼30 kW/cm^2. Both the conventional Raman and TERS measurement signals follow the same optical path back to the detector. AFM measurements were performed on an AIST-NT Omegascope. For TERS measurements, a mirror switch was used to send the same excitation laser to a set of external mirrors that illuminate the AFM tip in AIST-NT Omegascope. A 20× side objective side illuminates our AFM tip at an angle of 30 deg relative to the surface of the sample with a spot size of ∼5 μm and an incident laser power of ∼13 kW/cm^2. Because the sample stage moves instead of the tip when doing AFM, optical alignment is maintained throughout. TERS Raman spectra were collected using tapping mode configuration of the AFM with various oscillation amplitudes.

SEM images of TERS tips were obtained using a Zeiss Supra 40 V SEM.

RSoft DiffractMod software package was used to perform EM simulations. The DiffractMod package uses a combination of rigorous coupled wave analysis (RCWA) with modal transmission line (MTL) theory. In the simulation, five Fourier harmonics were used when modeling the simulation geometry.

■ ASSOCIATED CONTENT

Supporting Information

Additional information on transport and bandstructure calculations, strain calculations, electromagnetic simulations, and more detailed Raman shift analysis. The Supporting Information is available free of charge on the ACS Publications website at DOI: 10.1021/acs.nanolett.5b00176.

■ AUTHOR INFORMATION

Corresponding Author

*(E.T.Y.) E-mail: ety@ece.utexas.edu. Telephone: +1.512.232.5167. Fax: +1.512.471.8969.

Author Contributions

Z.Z., E.T., and E.T.Y. conceived of and designed the experiment. Z.Z. conducted all Raman experiments and electromagnetic simulations. Z.Z. and E.T.Y. developed the analysis of the data. D.C.D grew the core/shell nanowires and performed TEM, EDX, and electrical characterization of the nanowires. Z.Z. and E.T.Y. cowrote the manuscript. All authors commented and contributed to the work.

DOI: 10.1021/acs.nanolett.5b00176
Nano Lett. 2015, 15, 4303−4310

Funding

Part of this work was supported by the U.S. National Science Foundation (DMR-1311866, DMR-0846573) and the Judson S. Swearingen Regents Chair in Engineering at the University of Texas at Austin.

Notes

The authors declare no competing financial interest.

REFERENCES

(1) *Modern Techniques in Raman Spectroscopy*; John Wiley & Sons: New York, 1996).
(2) Smith, E.; Dent, G. *Modern Raman Spectroscopy—A Practical Approach*; John Wiley & Sons: New York, 2005.
(3) Stöckle, R. M.; Suh, Y. D.; Deckert, V.; Zenobi, R. Nanoscale chemical analysis by tip-enhanced Raman spectroscopy. *Chem. Phys. Lett.* **2000**, *318*, 131−136.
(4) Anderson, M. S. Locally enhanced Raman spectroscopy with an atomic force microscope. *Appl. Phys. Lett.* **2000**, *76*, 3130.
(5) Hayazawa, N.; Inouye, Y.; Sekkat, Z.; Kawata, S. Metallized tip amplification of near-field Raman scattering. *Opt. Commun.* **2000**, *183*, 333−336.
(6) Xiang, J.; Lu, W.; Hu, Y.; Wu, Y.; Yan, H.; Lieber, C. M. Ge/Si nanowire heterostructures as high-performance field-effect transistors. *Nature* **2006**, *441*, 489−493.
(7) Nah, J.; Dillen, D. C.; Varahramyan, K. M.; Banerjee, S. K.; Tutuc, E. Role of confinement on carrier transport in Ge-Si(x)Ge(1-x) core-shell nanowires. *Nano Lett.* **2012**, *12*, 108−112.
(8) Xiang, J.; Vidan, A.; Tinkham, M.; Westervelt, R. M.; Lieber, C. M. Ge/Si nanowire mesoscopic Josephson junctions. *Nat. Nanotechnol.* **2006**, *1*, 208−213.
(9) Sau, J. D.; Tewari, S.; Das Sarma, S. Experimental and materials considerations for the topological superconducting state in electron- and hole-doped semiconductors: Searching for non-Abelian Majorana modes in 1D nanowires and 2D heterostructures. *Phys. Rev. B* **2012**, *85*, 064512.
(10) Björk, M. T.; Thelander, C.; Hansen, A. E.; Jensen, L. E.; Larsson, M. W.; Wallenberg, L. R.; Samuelson, L. Few-Electron Quantum Dots in Nanowires. *Nano Lett.* **2004**, *4*, 1621−1625.
(11) Hu, Y.; Churchill, H. O. H.; Reilly, D. J.; Xiang, J.; Lieber, C. M.; Marcus, C. M. A Ge/Si heterostructure nanowire-based double quantum dot with integrated charge sensor. *Nat. Nanotechnol.* **2007**, *2*, 622−625.
(12) Li, D.; Wu, Y.; Kim, P.; Shi, L.; Yang, P.; Majumdar, A. Thermal conductivity of individual silicon nanowires. *Appl. Phys. Lett.* **2003**, *83*, 2934.
(13) Chen, R.; Hochbaum, A. I.; Murphy, P.; Moore, J.; Yang, P.; Majumdar, A. Thermal Conductance of Thin Silicon Nanowires. *Phys. Rev. Lett.* **2008**, *101*, 105501.
(14) Hochbaum, A. I.; Chen, R.; Delgado, R. D.; Liang, W.; Garnett, E. C.; Najarian, M.; Majumdar, A.; Yang, P. Enhanced thermoelectric performance of rough silicon nanowires. *Nature* **2008**, *451*, 163−167.
(15) Boukai, A. I.; Bunimovich, Y.; Tahir-Kheli, J.; Yu, J. K.; Goddard, W. A.; Heath, J. R. Silicon nanowires as efficient thermoelectric materials. *Nature* **2008**, *451*, 168−171.
(16) Schmidt, V.; McIntyre, P.; Gösele, U. Morphological instability of misfit-strained core-shell nanowires. *Phys. Rev. B* **2008**, *77*, 235302.
(17) Liang, Y.; Nix, W. D.; Griffin, P. B.; Plummer, J. D. Critical thickness enhancement of epitaxial SiGe films grown on small structures. *J. Appl. Phys.* **2005**, *97*, 043519.
(18) Grönqvist, J.; Søndergaard, N.; Boxberg, F.; Guhr, T.; Åberg, S.; Xu, H. Q. Strain in semiconductor core-shell nanowires. *J. Appl. Phys.* **2009**, *106*, 053508.
(19) Cerdeira, F.; Cardona, M. Effect of Carrier Concentration on the Raman Frequencies of Si and Ge. *Phys. Rev. B* **1972**, *5*, 1440−1454.
(20) Olego, D.; Cardona, M. Self-energy effects of the optical phonons of heavily doped p-GaAs and p-Ge. *Phys. Rev. B* **1981**, *23*, 6592.
(21) Zhang, S.; Lopez, F. J.; Hyun, J. K.; Lauhon, L. J. Direct detection of hole gas in Ge-Si core-shell nanowires by enhanced Raman scattering. *Nano Lett.* **2010**, *10*, 4483−4487.
(22) Wagner, R. S.; Ellis, W. C. Vapor-Liquid-Solid Mechanism of Single Crystal Growth. *Appl. Phys. Lett.* **1964**, *4*, 89.
(23) Dillen, D. C.; Varahramyan, K. M.; Corbet, C. M.; Tutuc, E. Raman spectroscopy and strain mapping in individual Ge-Si_xGe_{1-x} core-shell nanowires. *Phys. Rev. B* **2012**, *86*, 045311.
(24) Raychaudhuri, S.; Yu, E. T. Calculation of critical dimensions for wurtzite and cubic zinc blende coaxial nanowire heterostructures. *J. Vac. Sci. Technol. B: Microelectron. Nanom. Struct.* **2006**, *24*, 2053.
(25) Pinczuk, A.; Burstein, E.; Cardona, M. *Light Scatt. Solids* **1975**, 23−78.
(26) Abstreiter, G., Cardona, M.; Pinczuk, A. In *Light Scattered Solids IV* (Cardona, M., Guntherodt, G., Eds.; Springer-Verlag: Berlin, 1984; pp 5−145.
(27) Fano, U. Effects of Configuration Interaction on Intensities and Phase Shifts. *Phys. Rev.* **1961**, *124*, 1866−1878.
(28) Cerdeira, F.; Fjeldly, T. A.; Cardona, M. Effect of Free Carriers on Zone-Center Vibrational Modes in Heavily Doped p-type Si. II. Optical Modes. *Phys. Rev. B* **1973**, *8*, 4734−4745.
(29) Palik, E. D. *Handbook of Optical Constants of Solids*; Academic Press: San Diego, CA, 1998.
(30) Weber, W. Adiabatic bond charge model for the phonons in diamond, Si, Ge, and α-Sn. *Phys. Rev. B* **1977**, *15*, 4789−4803.

DOI: 10.1021/acs.nanolett.5b00176
Nano Lett. 2015, 15, 4303−4310